Modeling of Solid-State Polycondensation. I. Particle Models

FREDERICK K. MALLON, W. HARMON RAY

Department of Chemical Engineering, University of Wisconsin, Madison, Wisconsin 53706

Received July 1997; accepted 9 September 1997

ABSTRACT: A comprehensive model has been developed to handle the reactions in polymers undergoing polycondensation reactions in the solid state. The polymer crystalline fraction is modeled as containing only repeat units, thus concentrating end groups and condensate in the amorphous fraction. In addition, by using a general framework for the equations, many previously neglected effects are included; for example, variable crystallinity and gas phase mass transfer effects. This model is compared to PET and nylon reaction data with good results. © 1998 John Wiley & Sons, Inc. J Appl Polym Sci 69: 1233–1250, 1998

Key words: solid-state reactions; polymer reaction engineering; nylon; PET

INTRODUCTION

Because degradation reaction rates, in general, increase at a faster rate with temperature than do chain-building reaction rates, the polymerization of PET and nylon is carried out at lower temperatures in the solid state to produce high molecular weights. In general, the reaction is carried out from prepolymer pellets of 10–20,000 molecular weight at a temperature within 40°C of the melting transition.[1] The gas phase of such a reactor is either flushed with an inert gas or maintained at a vacuum so as to give low condensate partial pressures.

Previous modeling of solid-state reactions has used one of three basic approaches: straight empirical fits of the data, assuming the reaction was limited by the diffusion rates of polymer chains, or assuming that the reaction was limited by the diffusion rates of small molecules. Several authors have correlated their reaction data with empirical functions that have reaction rates that are nonlinear in time.[2–4] Due to the nonautonomous properties of this method and the difficulty in applying fitted constants to other work, this type of model has limited value.

In the second approach, the diffusion of the polymer chains is assumed to be the limiting step.[2,5–7] Proponents of this idea assume that chain ends must diffuse to find each other before reacting. This mechanism does not allow for small molecule diffusion limitations; meaning that particle size has no effect on the polymerization (as one often sees, especially with PET). Furthermore, Warner and Lee[8] argue that this implies a polymer chain end diffusivity that is too small; a result confirmed by our own work.[9]

Finally, because particle size often has a large effect on reaction rates, many modeling studies (including this one) consider the reaction to be limited by condensate diffusion. Briefly, the polycondensation reaction can be written as eq. (1):

$$P_m + P_n \leftrightarrow P_{m+n} + C \qquad (1)$$

The finite equilibrium constant for eq. (1) means that, to achieve high molecular weights, the small molecule (C) must be removed. This situation leads to condensate diffusion limitations. This diffusion limit is different from the

Correspondence to: W. H. Ray.

Journal of Applied Polymer Science, Vol. 69, 1233–1250 (1998)
 CCC 0021-8995/98/061233-18

Table I PET Solid-State Experiments in a Fluidized Bed

Particle size	Between #10 and #12 sieves (about 1 mm)
Particle preparation method	As supplied polymer ground to particle size above. Initial molecular weight = 14,400
Crystallization steps	See text below
Gas flow rate/superficial velocity	17–17.5 standard liters per minute (about 2.4 m/s)
Purge type and purity	$N_2 > 99.99\%$, $O_2 < 5$ ppm, $H_2O < 3$ ppm
Time from beginning of heating to experiment start (heat-up time)	25 min (because of crystallization)
Time from end of experiment until polymer bed is 60°C (cool-down time)	10 min

case of polymer chain diffusion in that here the small molecule (condensate) diffuses to the particle surface and evaporates. Here, the diffusion length scale is about 1 mm, instead of $\sim$ 1 nm. when the diffusion rate of polymer chains is limiting.

Most of the work with the models described above has been with PET.[10–14] Ravindranath and Mashelkar[12] described solid-state polymerization of PET by assuming that all polymer chains had only ethylene glycol ends, that the varying crystallinity did not affect polymerization or diffusion, and that the effect of mass transfer to the gas phase could be handled by merely setting a fixed concentration at the particle boundary. Tang et al.[14] relaxed the first assumption; however, this added three more fitted parameters (total of six). Their model would have required 10 parameters if nonisothermal polymerization were to be considered.

In this work, similar ideas will be employed, but, by using a more fundamental approach, many fewer constants will be needed. In the present article, a particle model will be developed and compared with experimental data. In the sequel, the overall reactor behavior will be modeled and reactor design issues addressed.

EXPERIMENTAL DETAILS

The experimental portion of this work is a series of solid-state polymerizations in a small fluidized bed. The conditions of Table I are the base case for the experiments reported in the text; all deviations from these conditions are noted. The experimental apparatus is shown in Figure 1 and more fully described elsewhere.[9,15] For the experiments discussed here, no microwave energy was used.

For each polymerization, the reactor was charged with pellets. The bed was purged with high purity nitrogen for 2 min (flow rate was approximately 3 L/min). The temperature was increased in steps to precrystallize the PET to avoid sticking at reaction temperature. After purging, the heaters were turned on, the inlet temperature setpoint set at 132°C, and the flow rate was increased to 17 L/min. This first crystallization step was allotted 8 min. Next, the temperature set point was raised to 190°C for 10 min (the second crystallization step). Finally, the temperature set point was raised to the reaction temperature. When the temperature settled to within 5°C of the set point, the experiment was considered to have begun, i.e., reaction time was counted from this point. Time from the beginning of heating to the zero time for the experiment was about 26 min. The resulting polymer samples were examined by FTIR according to the method of Ward and others[16–18]; this generates values for the various end group concentrations as well as the number-average molecular weight.

The conditions of Table II are the base case for

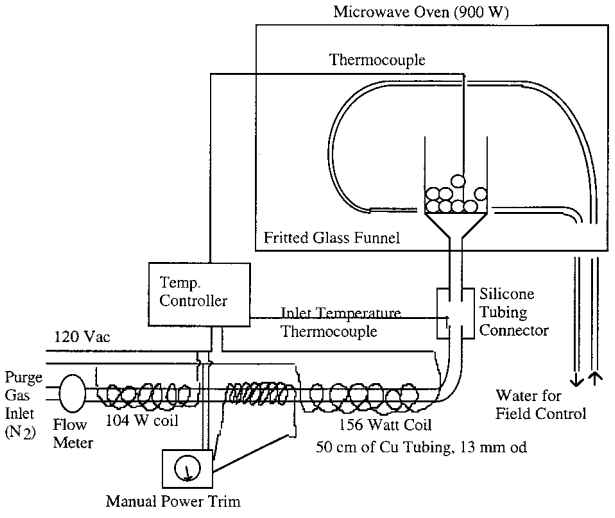

Figure 1 Solid-state reactor schematic.

Table II Nylon 66 Solid-State Experiments

Particle size	About 15 mg (±20%)
Particle preparation method	Depolymerized to 4300 molecular weight (see text below) (DuPont nylon)
Crystallization steps	None
Gas flow rate/superficial velocity	17–17.5 standard liters per minute (about 2.4 m/s)
Purge type and purity	$N_2 > 99.99\%$, $O_2 < 5$ ppm, $H_2O > 3$ ppm
Bed weight for each experiment	0.9 g
Heat-up procedure	See text below
Time from beginning of heating to experiment start (heat-up time)	10 min
Time from end of experiment until polymer bed is 60°C (cool-down time)	10 min

the nylon experiments reported in this work; all deviations from these conditions are noted. Where some explanation of table entries is necessary, see the text following the table.

Nylon 66 particles were graciously provided by DuPont. The initial molecular weight was approximately 20,000. Because Gaymans et al.[2] found interesting behavior when starting with lower molecular weight particles, the particles were depolymerized to about 4300 molecular weight prior to the solid-state experiments. This was done in a stainless steel vessel with 45 g of nylon particles and 10 mL of water. The oxygen was removed with a nitrogen purge, the vessel sealed, and the vessel was placed in an oven at 190–200°C. The reaction was allowed to proceed for about 15 h. Following this, the vessel was cooled and the polymer removed.

For each polymerization, the reactor was charged with pellets. The bed of nylon 66 particles was purged with high purity nitrogen for 2 min (flow rate was approximately 3 L/min). The heaters were then turned on and the inlet temperature set point was set at the desired temperature. When the inlet temperature reached 90–100°C, the flow rate was increased to 17 L/min. By this method, the resin bed temperature increased rapidly. When the temperature was within 5°C of the reaction temperature, the experiment was considered to have begun, i.e., reaction time was counted from this point. Time from the beginning of heating to the zero time for the experiment was about 10 min. The number-average molecular weight was analyzed by titration in a solution of about 0.08 g LiCl in 10 mL of CF_3CH_2OH.

Melt Polymerization Kinetics of PET and Nylon

Before addressing the special issues of solid-state polymerization, we shall review our models for melt polymerization. These melt models will be employed in the amorphous phase of the polymer particles for solid-state polymerization. For PET, the reactions (Fig. 2) and kinetic constants are adapted from Ravindranath and Mashelkar[19] (Table III).

The nylon melt model will be that of Mallon and Ray.[20] In that work, a model for nylon melt thermodynamics is assumed that explains the variable equilibrium constant. In addition, an increasing dielectric constant is assumed to reduce the apparent rate constant. Because water increases the system dielectric constant, increased water contents depress the observed rate constant.

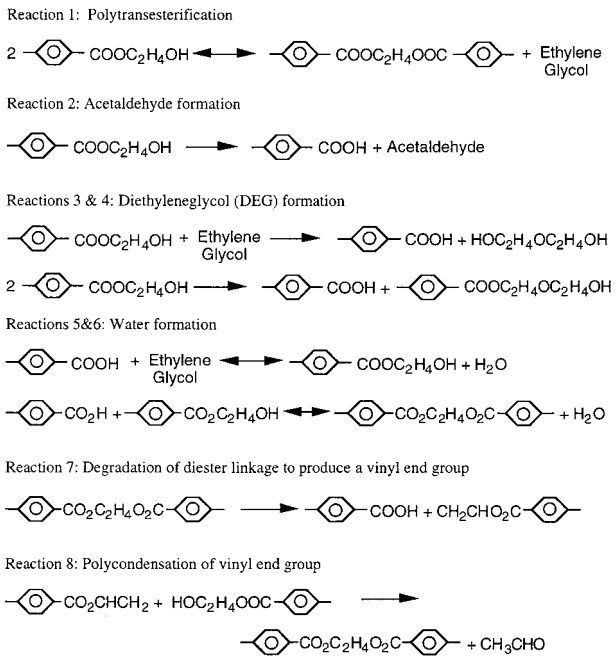

Figure 2 Reaction mechanisms for PET (Ravindranath et al.[19]).

Table III Converted PET Kinetic Constants of Ravindranath et al.[19]

Reaction (see Fig. 2)	Polycondensation Eq. (1)	Acetaldehyde Formation Eq. (2)	DEG Formation Eqs. (3) and (4)	Esterification Eqs. (5) and (6)	Diester Group Degradation Eq. (7)	Polycondensation of Vinyl End Group Eq. (8)
Activation energy kcal/mol	18.5	29.8	Not used	17.6	37.8	18.5
Frequency factor kg/mol/h[a]	9.91×10^7	5.0×10^9	Not used	1.52×10^8	2.2×10^{11}	9.91×10^7
Equilibrium Constant	0.5	—	—	1.25	—	—

[a] Reactions 2 and 7 are unimolecular and have units of h^{-1}.

CRYSTALLIZATION

An important aspect of solid-state polymerization is the presence of crystalline polymer, which reacts very slowly and forms obstructions lengthening the diffusion path of the condensate out of the particle.

The rate of crystallization is often described by the Avrami equation [eq. (2)], yielding the nonautonomous initial period of crystallization. The nonlinear, autoacceleration character of the crystallization comes from the changing surface area available for further crystallization; as more material crystallizes, an even greater area for growth results.

$$(1 - \chi_c) = \exp(-kt^n),$$

n a function of nucleation and growth type (2)

However, the Avrami equation does not describe the entire course of the crystallization. As can be seen from Figure 3, there is a definite change in slope even though eq. (2) states that all data points[21] should be fitted with a single line on a semilog scale. This change in slope is a demarcation between primary and secondary crystallization. Several authors have attempted to describe the two regimes with one equation[22–24]; however, the methods amount mostly to more complicated empirical expressions. The crystallization rate accelerates because as the overall crystalline fraction increases, the area available for crystallization increases. However, as higher degrees of crystallinity are achieved, the material available for crystallization is reduced, and the area available for crystallization stops growing geometrically. This causes a fundamental change in the crystallization kinetics. This second stage is modeled in more detail below.

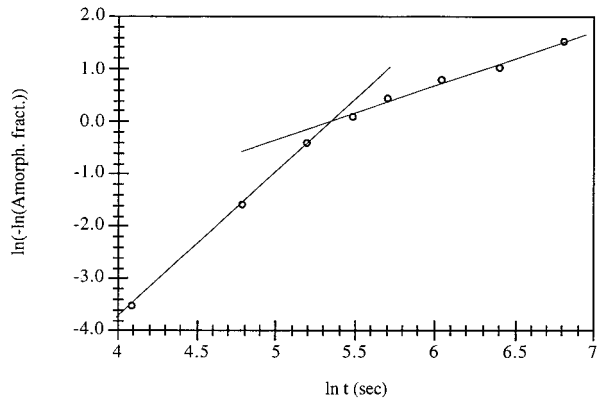

Figure 3 PET crystallization (primary and secondary), data of Jabarin[21] (Goodyear 5041X PET at 200°C).

MODEL FOR SOLID-STATE REACTIONS—ASSUMPTIONS

Following the works of Gostoli et al.,[25] Zimmerman,[26] and Meyer,[27] a general model for the polymerization of condensation polymers in the solid state is proposed in this work. The following assumptions are made.

1. Polymer end groups, monomers, condensate, and catalysts exist exclusively in the amorphous phase (Fig. 4). This idea assumes that, upon crystallization, these species are expelled from the ordered crystalline phase. This assumption is similar to the observed freezing behavior in low molecular weight systems where each solid component, in general, forms a pure phase. So, as salt water freezes, the solid formed is pure H_2O, not a mixture of NaCl and H_2O. The molar concen-

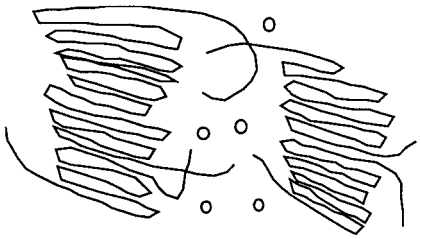

Figure 4 Fractionation between crystalline and amorphous phases.

trations of noncrystallizing components will then increase because their accessible volume is now only in the amorphous phase.

$$C_{\text{amorphous}} = C_{\text{overall}}/(1 - \chi_c) \qquad (3)$$

Crystallization-induced fractionation leads to dramatic shifts in the apparent kinetics and equilibria. Because the crystalline regions reject the condensate and end groups, the local concentrations in the amorphous phase increase. This leads to higher observed reaction rates because these reactions are second order and higher. Similarly, the equilibrium also shifts to higher conversions and chain length. (Both end group and condensate concentrations increase; however, because the end group concentration is squared in the equilibrium expression, this leads to higher conversions.)

The assumption also affects the driving force for mass transfer. The increase in local concentration of condensate [eq. (3)] means that if this phase is in equilibrium with the gas phase, more condensate will flow to the gas upon crystallization of the polymer.

2. The reaction chemistry in the amorphous phase is the same as in the melt. This is assumed because melting only affects the crystalline regions of the polymer; the amorphous region is continuous with the melt. The assumption of melt kinetics then allows the direct application of melt kinetic expressions for the amorphous phase of a solid semicrystalline polymer. Because melt reactions have often been studied more comprehensively in the literature, this assumption reduces the modeling load considerably.
3. No reactions occur in the crystalline phase. The crystallites are so compact that molecular motions necessary for reaction are very improbable. Additionally, the chain ends, condensate, and catalysts are, by assumption 1, not present in this phase. This further reduces the probability of reaction.
4. The free-volume model of Fujita[28] for diffusivity is not necessary. His model is most useful close to the glass transition due to the rapidly changing free volume, but close to the melting point the free volume is not changing as quickly. All diffusivities observed in this work were easily fit with the common activation energy model [eq. (4)] because solid-state polymerizations are generally carried out close to the melting point, not the glass transition point.

$$D_o = A_d \exp(-B_d/RT) \qquad (4)$$

This also removes the need for estimates of the various parameters needed for the free volume model.

5. The observed small molecule diffusivity is proportional to the amorphous fraction.

$$D = D_o(1 - \chi_c) \qquad (5)$$

Michaels et al.[29] and Yoon et al.[30] provide data that suggest this proportionality holds for PET. In addition, because the free-volume model was not used, the use of the extension of Kulkarni et al.[31] to describe the effect of crystallization is not appropriate. By analogy with conventional effective diffusivity notions,[32] the diffusivity could even be reduced further by a tortuousity factor to account for the increase in diffusion distance because the polymer crystallites obstruct the diffusion path.

Because of the interconnectedness of crystallinity and diffusivity, the dynamic changes in crystallinity are modeled as well. Here, crystallization reduces the diffusivity which, in turn, reduces the mass transport rate.

6. We assume that the Avrami Equation [eq. (2)] is an adequate representation of the initial stage of crystallization. However, this stage only represents a short time interval; hence, we assume that the crystallization rate is proportional to the crystallizable amorphous fraction.

$$\frac{d\chi_c}{dt} = (\chi_{\max} - \chi_c)k_c,$$

$$k_c = A_c \exp(B_c/RT) \qquad (6)$$

$$\chi_{\max} = A + B(T - T_o) \qquad (7)$$

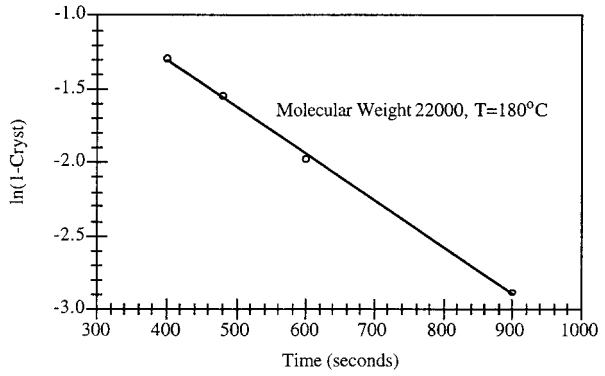

Figure 5 Secondary crystallization of ICI PET, data of Jabarin.[21]

This assumption is based on the primary crystallization step occurring quickly compared to the reactor residence time. From Figure 3, one can see that the change in slope, signifying the transition from primary to secondary crystallization, on an Avrami plot for PET occurs at about 4 min. By comparison, reactor residence times are generally of the order of many hours. To add further plausibility, Figure 5 shows the secondary crystallization rate to be linear in crystalline fraction—in agreement with eq. (6). However, the adequacy of this simple model will be discussed in more detail below.

Figure 6 shows that the molecular weight of PET (shown as intrinsic viscosity) seems to have little effect on the rate of crystallization at temperatures 210°C and higher. Because solid-state polycondensation is generally restricted to these temperatures, the rate of crystallization is modeled as being independent of molecular weight.

7. The polymer particles are assumed to have a uniform temperature. This assumption is based on the thermal diffusion times in the reactor pellets

$$\left(\frac{R^2}{\alpha} = 10 \text{ s}\right)$$

being small compared to the residence time (often 20 h) and the time required for diffusion (on the order of 10 h).

The Particle Model

The particle model variables can be divided into two types: those that are subject to diffusion and mass transfer to the gas phase, and those that are not. In the equations that follow, the concentrations are expressed in units of mol/kg. This makes mol and mass balances straightforward. The set of variables subject to diffusion is composed of the concentrations of solvent, condensate, and monomers and is shown generally as

$$\frac{\partial(MC_v)}{\partial t} = MR_v + MD\nabla^2 C_v \tag{8}$$

or rearranging under conditions of changing mass

$$\frac{\partial C_v}{\partial t} = R_v + D\nabla^2 C_v - \frac{C_v}{M}\frac{dM}{dt} \tag{9}$$

Here, C_v denotes the concentration of a "volatile" state and R_v the rate of generation of C_v by reaction. The volatile states refer to components that can diffuse and evaporate. Examples of these are water and monomers. The second set of variables are described by a similar equation with the diffusion term removed:

$$\frac{\partial(MC_n)}{\partial t} = MR_n \tag{10}$$

or rearranging under conditions of changing mass

$$\frac{\partial C_n}{\partial t} = R_n - \frac{C_n}{M}\frac{dM}{dt} \tag{11}$$

where, as before, C_n denotes the concentration of "nonvolatile" states and R_n the rate of generation of C_n by reaction. As mentioned above, the reaction term is the same as for the melt (assumption

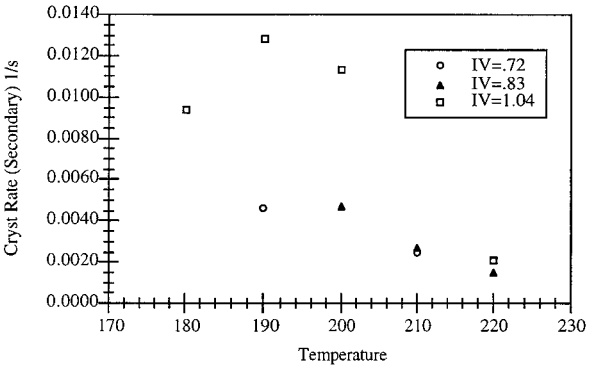

Figure 6 Molecular weight [shown as Intrinsic Viscosity (IV)] effect on PET crystallization, data of Jabarin.[21]

2); however, the concentrations are adjusted to account for the end groups and condensate being concentrated in the amorphous phase (assumption 1). Additionally, because the reaction rate used in eqs. (9) and (11) is on a total particle mass basis, the rate must be multiplied by the amorphous fraction because the reaction is only occurring in the amorphous fraction. Hence,

$$R_v \text{ or } R_n = (1 - \chi_c) g_{v \text{ or } n} \times (C_{v,\text{amorph}}, C_{n,\text{amorph}}, \quad T) \quad (12)$$

The function g is either the PET reaction function of Ravindranath and Mashelkar[19] or the nylon one of Mallon and Ray.[20]

There are three possible assumptions regarding the boundary conditions for eq. (9) [because eq. (11) involves no spatial variation, only an initial condition is needed). The center of the particle should obviously have a no flux condition

$$\left(\frac{\partial C_v}{\partial_x} = 0 \right)$$

Equation (13) describes the mass transport at the surface.

$$R_{MT,v} = k_m (f_{\text{solid},v} - P_{\text{gas},v}) \quad (13)$$

where $f_{\text{solid},v}$ represents the fugacity of the volatile species at the particle surface.

The three different limiting cases lead to three different methods for calculating the other boundary condition for eq. (9). In the first, no mass transfer occurs ($k_m = 0$); this sets

$$\frac{\partial C_v}{\partial_x} = 0$$

at the surface also. In the second, mass transfer at the surface is balanced by diffusion to the surface.

$$-\rho D \nabla C_v|_{\text{surface}} = R_{MT,v}$$

This condition allows the gas and solid phases to be in equilibrium if the gas phase condensate concentration is sufficiently high that the driving force for mass transfer goes to zero. This option allows nonzero concentrations of condensate at the surface while avoiding the artificial statement of a fixed finite concentration.[12,13] In the third, the concentration of the diffusant at the interface between the solid and gas phases is assumed to be that in equilibrium with the gas phase concentration ($k_m = \infty$ and $f_{\text{solid},v} = P_{\text{gas},v}$). This amounts to assuming that the mass transfer resistance is completely inside the polymer particle. If one assumes very low gas phase concentrations, then the amorphous phase concentrations of volatile species at the particle surface will be near zero.

To reduce and simplify the system of equations further, the polymer particles are assumed to be monodisperse in size. This is reasonable because, the particles are generally formed mechanically by extrusion and subsequent cutting. In addition, the particles are assumed to have one of three principal geometries (flake, cylinder, or sphere).

Because of possible diffusion limitations,[10,11] concentration gradients for the volatile species can develop across the particle radius. These concentration gradients were computed using collocation methods that convert the volatile species partial differential equations to a set of ordinary differential equations. More details on the method may be found in Mallon.[9]

The basic structure of the kinetics used in the model is based on the thesis of Jacobsen,[33] who characterized the polymerization through the method of moments. The method of moments is a particularly efficient way of reducing the number of equations to a tractable set. Table III gives the kinetic and equilibrium constants used for PET simulation (the reaction number then becomes the subscript for the kinetic and equilibrium constant for each reaction). Tables IV and V give the explicit equations for modeling solid-state polymerization of PET and nylon 66, respectively.

PET SOLID-STATE POLYMERIZATION—ANALYSIS

An interesting feature of the kinetics of Ravindranath et al.[19] is the second-order behavior in the kinetic expressions. Because Flory[34] found third-order kinetics at high conversions for polyesters, Ravindranath et al. implicitly lump the catalyst concentration into the rate expression. Thus, all the rate constants in Table III assume some catalyst concentration. Such an expression also means that the catalyst dominates the catalyzing influence of the carboxyl ends. Because the reaction chemistry avoids carboxyl ends and because this work is concerned with solid-state polycondensation that is conducted at higher molecular

Table IV Equations for PET

$$\frac{\partial \lambda_0}{\partial t} = (1-\chi_c)\left(-k_6\frac{C_A C_B}{(1-\chi_c)^2} + \frac{k_6}{K_6}\frac{WL}{(1-\chi_c)} + k_7 L - k_8\frac{C_{A'}C_A}{(1-\chi_c)^2}\right) + D_{\text{e.g.}}\nabla^2\frac{C_{\text{e.g.}}}{(1-\chi_c)} - \frac{\lambda_0}{M}\frac{\partial M}{\partial t}$$

$$\frac{\partial \lambda_{1,1}}{\partial t} = (1-\chi_c)\left(-k_2\frac{(C_A - 2C_{\text{e.g.}})}{(1-\chi_c)} - k_7 L\right) + D_{\text{e.g.}}\nabla^2\frac{C_{\text{e.g.}}}{(1-\chi_c)} - \frac{\lambda_{1,1}}{M}\frac{\partial M}{\partial t}$$

$$\frac{\partial \lambda_{1,2}}{\partial t} = -\frac{\lambda_{1,2}}{M}\frac{\partial M}{\partial t}, \quad \lambda_1 = \lambda_{1,1} + \lambda_{1,2}$$

$$\frac{\partial C_A}{\partial t} = (1-\chi_c)\left(-k_2\frac{(C_A - 2C_{\text{e.g.}})}{(1-\chi_c)} - k_6\frac{C_A C_B}{(1-\chi_c)^2} + \frac{k_6}{K_6}\frac{WL}{(1-\chi_c)} - k_8\frac{C_{A'}C_A}{(1-\chi_c)^2}\right) + 2D_{\text{e.g.}}\nabla^2\frac{C_{\text{e.g.}}}{(1-\chi_c)} - \frac{C_A}{M}\frac{\partial M}{\partial t}$$

$$\frac{\partial C_{A'}}{\partial t} = (1-\chi_c)\left(k_7 L - k_8\frac{C_{A'}C_A}{(1-\chi_c)^2}\right) - \frac{C_{A'}}{M}\frac{\partial M}{\partial t}$$

$$\frac{\partial C_B}{\partial t} = (1-\chi_c)\left(k_2\frac{(C_A - 2C_{\text{e.g.}})}{(1-\chi_c)} - k_6\frac{C_A C_B}{(1-\chi_c)^2} + \frac{k_6}{K_6}\frac{W}{(1-\chi_c)}L + k_7 L\right) - \frac{C_B}{M}\frac{\partial M}{\partial t}$$

$$\frac{\partial W}{\partial t} = (1-\chi_c)\left(k_6\frac{C_A C_B}{(1-\chi_c)^2} - \frac{k_6}{K_6}\frac{W}{(1-\chi_c)}L\right) + D_W\nabla^2\frac{W}{(1-\chi_c)} - \frac{W}{M}\frac{\partial M}{\partial t}$$

$$\frac{\partial C_{\text{e.g.}}}{\partial t} = (1-\chi_c)\left(k_1\frac{(C_A - 2C_{\text{e.g.}})^2}{(1-\chi_c)^2} - \frac{k_1}{K_1}L\frac{2C_{\text{e.g.}}}{(1-\chi_c)} - k_6\frac{2C_{\text{e.g.}}C_B}{(1-\chi_c)^2} + \frac{k_6}{K_6}\frac{W(C_A - 2C_{\text{e.g.}})}{(1-\chi_c)^2}\right) + D_{\text{e.g.}}\nabla^2\frac{C_{\text{e.g.}}}{(1-\chi_c)} - \frac{C_{\text{e.g.}}}{M}\frac{\partial M}{\partial t}$$

$$\frac{\partial M}{\partial t} = 0.062\,D_{\text{e.g.}}\nabla^2\frac{C_{\text{e.g.}}}{(1-\chi_c)} + 0.018\,D_w\nabla^2\frac{C_w}{(1-\chi_c)} + 0.044\left(k_2(C_A - 2C_{\text{e.g.}}) + k_8\frac{C_{A'}C_A}{(1-\chi_c)}\right)$$

$$L = \frac{1 - \sum^{w_{i,\text{amorphous}}}_{i=\text{condensates, monomers}}}{1 - \sum^{w_{i,\text{overall}}}_{i=\text{condensates, monomers}}}(\lambda_1 - \lambda_0)$$

For modeling, $D_w = D_{\text{e.g.}}$. Concentrations shown are overall concentrations (mol/kg); eq. (3) has already been used to convert the quantities to amorphous phase concentration. Crystallinity is calculated with eq. (6). Reactions 3 and 4 of Figure 2 are neglected. The generated acetaldehyde is assumed to volatilize instantly in the mass equation. Reactions 5 and 6 are combined by assuming the equal reactivity hypothesis. Boundary conditions are discussed above.

weights, the catalyzing effect of the carboxyl ends is reduced from the already low value.

Clearly, the catalyst concentration can have a strong effect on the reaction rate for PET. Kokkalas et al.[35] varied the amount of Sb_2O_3 in small PET particles and found the rate of ester interchange to be first order with respect to the catalyst concentration. Kokkalas et al. observed a flattening in the reaction rate at higher catalyst concentrations. This effect, however, can be attributed to the reaction being carried out in the solid state. Because approximately 0.3-mm particles were used, the diffusion limitation will not be apparent when the catalyst concentration is low or zero, but at higher concentrations the reaction can become diffusion limiting again. The use of rate constants for a variety of catalyst concentrations (like the constants of Ravindranath et al.) is only valid under two circumstances then. First, particles are of sufficient size such that diffusion is limiting. At this point the details of the reaction become unimportant because the removal of the small molecules and the equilibrium constant determine the rate of molecular weight increase. This is the situation seen for many industrial polymerizations of PET. Second, if most processes operate with approximately the same concentration of the catalyst, then the catalyst concentration can be lumped with the rate constant to give the correct pseudosecond-order rate expression even for small particles.

PET SOLID-STATE POLYMERIZATION—MODELING

In 1986, Jabarin et al.[3] carried out a series of experiments with commercial, low molecular weight PET. Our PET solid-state model (Table IV) was able to fit Jabarin's experimental data by

Table V Equations for Nylon 66

$$\frac{\partial \lambda_0}{\partial t} = \frac{\partial \lambda_{1,1}}{\partial t} = \frac{\partial \lambda_{1,2}}{\partial t} = (1 - \chi_c)\left(-k_1 \frac{C_A C_B^2}{(1 - \chi_c)^3} + \frac{k_1}{K''} L W_f \frac{C_B}{(1 - \chi_c)}\right) - \frac{(\lambda_0, \lambda_{1,1}, \text{ or } \lambda_{1,2})}{M} \frac{\partial M}{\partial t}$$

$$\frac{\partial W}{\partial t} = -(1 - \chi_c)\left(-k_1 \frac{C_A C_B^2}{(1 - \chi_c)^3} + \frac{k_1}{K''} L W_f \frac{C_B}{(1 - \chi_c)}\right) + D_w \nabla^2 W_f - \frac{W}{M} \frac{\partial M}{\partial t}$$

$$K' = \frac{\left(\frac{W}{(1 - \chi_c)} - W_f\right)}{\left(A_{\text{tot}} - 2\frac{W}{(1 - \chi_c)} + 2W_f\right)^2 W_f}, \quad A_{\text{tot}} = L + \frac{C_B}{(1 - \chi_c)}$$

$$\frac{\partial M}{\partial t} = 0.018\, D_w \nabla^2 W_f$$

$$L = \frac{1 - \sum_{\substack{i=\text{condensates,} \\ \text{monomers}}} w_{i,\text{amorphous}}}{1 - \sum_{\substack{i=\text{condensates,} \\ \text{monomers}}} w_{i,\text{overall}}} (\lambda_1 - \lambda_0)$$

The kinetic constants are from Mallon and Ray[20] (the ρ^2 terms convert to a mass basis)

$$k_1 = 0.0071 \exp\left(-\frac{8578}{R}\left(\frac{1}{T} - \frac{1}{503.15}\right)\right)\exp\left(\frac{40716}{\varepsilon RT}\right)\rho^2 \text{kg}^2/\text{mol}^2\text{h},$$

$$K' = 1.78 \times 10^{-10} \exp\left(\frac{18300}{RT}\right)\rho^2 \text{kg}^2/\text{mol}^2$$

For details on the calculation of density, ρ, and dielectric constant, ε, for nylon 6 and 66, please consult Mallon and Ray.[20] Concentrations shown are overall particle concentrations (mol/kg); eq. (3) has already been used to convert to amorphous phase concentrations. (A_{tot}, W_f, and L are concentrations in the amorphous phase.) Crystallinity is assumed constant, and boundary conditions are discussed above.

adjusting just two parameters: the preexponential factor, and the activation energy for diffusion of ethylene glycol. This experimental data included results using prepolymers from both Goodyear and Firestone, and four different reaction temperatures for each prepolymer. Samples of the prepolymer pellets used by Jabarin et al. were graciously provided by E. A. Lofgren. Pellets were mostly short right cylinders with a slightly elliptical cross-section. Because the cylinders were of approximately the same length as the particle diameter, the pellets were modeled as spheres with a radius of 0.122 cm and 0.133 cm for the Goodyear and Firestone resins, respectively. These radii were determined as a weighted average over the measured dimensions.

$$r_{\text{avg}} = \sqrt{\frac{3}{\frac{1}{s_1^2} + \frac{1}{s_2^2} + \frac{1}{s_3^2}}} \tag{15}$$

This expression was used because the dimension affecting the diffusion is the square of the distance. The inverse relation was used to prevent the model from calculating too slow a diffusion rate if one dimension was very large. Because the dimensions were fairly similar, other averaging methods gave similar results.

Because PET is insoluble in appropriate solvents at room temperature, titration of end groups is not usually used to determine molecular weights, as is the case with nylon. Instead, intrinsic or inherent viscosity in more caustic solvents is used to find the viscosity average molecular weight. This procedure, however, introduces a systematic bias in predictions of the number-average molecular weight. Because most polycondensation models treat the reacting ends as the fundamental feature of the system, these models predict the number-average molecular weight. When a particle is first extruded, it has a molecular weight distribution close to the ideal most probable distribution because the mixing and the heat of the extruder are usually sufficient to cause enough redistributional interchanges if a nonuniform distribution had existed previously. How-

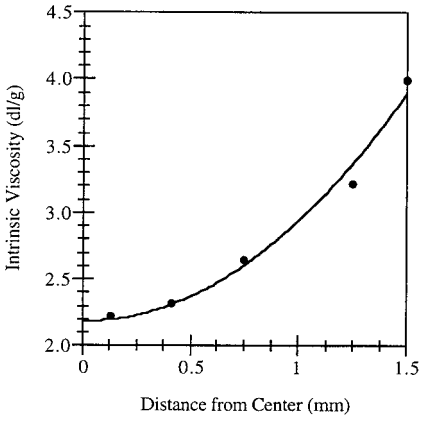

Figure 7 Intrinsic viscosity variation in a PBT particle, data of Buxbaum.[36]

ever, Figure 7 shows the variability of molecular weight in a PBT (polybutylene terephthalate) particle after solid-state polycondensation[36] (similar results should be expected for PET). Diffusion of 1,4 butanediol is sufficiently slow that outer regions experience lower local concentrations of the diffusant than do interior points. This feature for reactions close to equilibrium means that the effective polymerization rate at the exterior is greater. This nonuniformity in average molecular weight across the particle radius causes the overall polydispersity to increase dramatically. An increase in polydispersity means the ratio of the viscosity average molecular weight to the number average also increases. Because published accounts in the literature do not account for this (except Chen et al.[4]), number-average molecular weights at longer times calculated from intrinsic viscosity are too high.

A correct interpretation of intrinsic viscosity data requires explicit calculation of the number- and weight-average molecular weights. This was achieved in this work by the following procedure. First, the number-average molecular weight was calculated at each radial position (model of Table IV). Then, at each position in the particle, the polymer was assumed to have a most probable distribution (a polydispersity of 2) so as to generate the weight-average molecular weight. From this, an overall number- and weight-average molecular weight were determined for the particle, and a log normal distribution was used to find the viscosity average molecular weight. This was then used with eq. (16) (a Mark-Houwink expression) to determine the intrinsic viscosity. Equation (16) shows the relation between inherent viscosity and viscosity-average molecular weight for PET in a 60/40 phenol/tetrachloroethane mixture[37]; the multiplier of M_v is adjusted from the reference to account for the ratio of M_v/M_n for a most probable distribution.

$$\text{I.V.} = 5.46 \times 10^{-4} M_v^{0.68} \qquad (16)$$

Table VI Parameters for PET Simulation

Parameter	Value	Source
Kinetics	Table III	Ravindranath et al.[19]
Crystallizing rate	$3.6517 \times 10^{-14} \exp(23186/RT)$	This work
Maximum crystallinity	$0.390 + 0.0025\,(T - 470)$	This work
Diffusivity (water and ethylene glycol, cm^2/s)	$1.932 \times 10^{-6} \exp\left[\frac{-29670}{R}\left(\frac{1}{T} - \frac{1}{493}\right)\right]$	Data fit
Mass transfer	Volatile species conc. = 0 at surface	Assumption
Radial colloc. points number	4	Adequate from preliminary simul.
Temperature	Varies (see plots)	—
Initial carboxyl fraction of total end groups	0.32	Jabarin et al.
Energy balance	Isothermal	This work
Ratio of cryst. density/amorph. density	1.139	This work
Amorphous density	1.33	This work
Particle Shape	Sphere	Assumption
Particle Radius (cm)	0.133 (Firestone prepolymer) 0.122 (Goodyear prepolymer)	Measurement
Initial crystallinity	0.30	Assumption

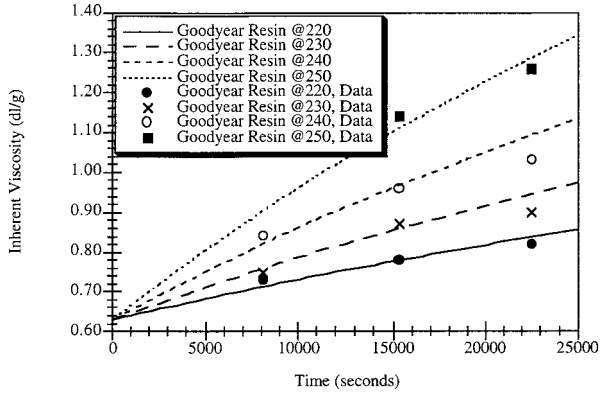

Figure 8 Solid-state polymerization of PET, fitted model versus data of Jabarin et al.[3] (Goodyear resin).

The data of Jabarin[21] were used to find the constants for eq. (6) (constants in Table VI).

$$\frac{d\chi_c}{dt} = (\chi_{\max} - \chi_c)k_c, \quad k_c = A_c \exp(B_c/RT) \quad (6)$$

Additionally, differential scanning calorimetry (DSC) was performed on other samples of PET to determine maximum extents of crystallinity at different temperatures. Using a value for the enthalpy of fusion of 26.9 kcal/mol,[38] the constants for eq. (7) were determined (Table VI).

$$\chi_{\max} = A + B(T - T_o) \quad (7)$$

For calculating the concentration of ethylene glycol in the particle, all of the mass transfer resistance was assumed to be in the interior of the particle. This assumption seems reasonable given the data of Chang,[11] where the particle size was shown to have a large influence on produced intrinsic viscosity. Under these conditions, the particle surface was assumed to be at the purge gas concentration (approximately zero).

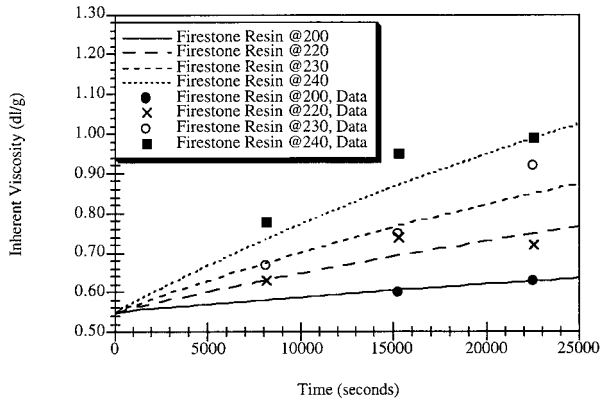

Figure 9 Solid-state polymerization of PET, fitted model versus data of Jabarin et al.[3] (Firestone resin).

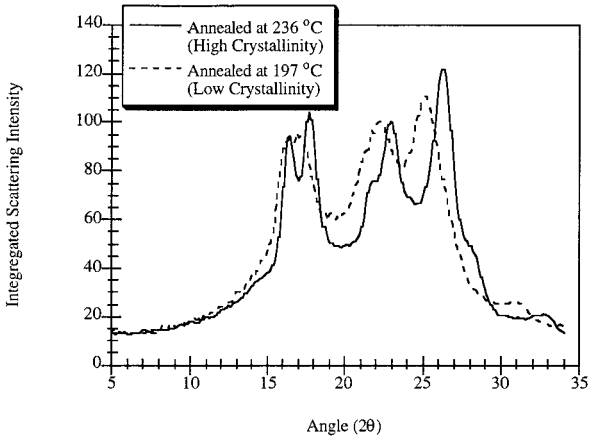

Figure 10 X-ray scattering peak shifts due to annealing of PET.

The Goodyear and Firestone data of Jabarin et al.[3] were fit by adjusting an Arrhenius expression for the condensate diffusivity. Using the conditions of Table VI, model predictions were compared to the data shown in Figures 8 and 9. The agreement is quite reasonable within the obvious variability of the data.

One possible objection to the data fit may be the tendency of the data to flatten out at higher conversions while the model predicts continued polymerization. There are several possible explanations for this trend. First, the diffusion constant was assumed linear in amorphous content. This is equivalent to saying that the diffusivity in a catalyst pellet is linear in the porosity. Such a

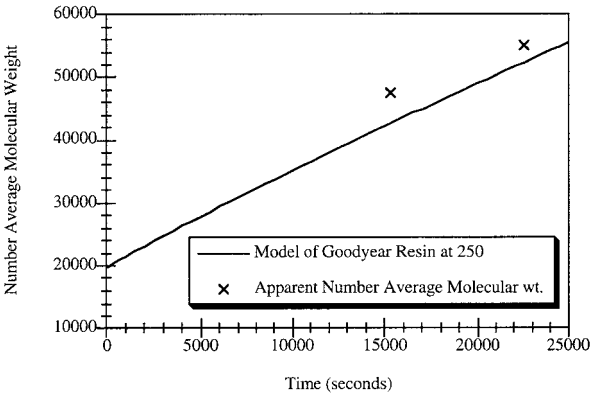

Figure 11 Effect of fitting intrinsic viscosity instead of number-average molecular weight for solid-state polymerization of PET, data of Jabarin et al.,[3] Goodyear resin at 250°C.

Table VII Effect of Initial Carboxyl Content on Fitted Diffusivity of Ethylene Glycol

Assumption	Diffusivity at 220°C (cm^2/s) (D_o)	Activation Energy for Diffusion (cal/mol)
Initial carboxyl fraction of total ends = 32%	1.93×10^{-6}	29,670
Initial carboxyl fraction of total ends = 0%	3.96×10^{-6}	27,005

statement is a good approximation at high porosities, but as the porosity decreases, the tortuousity increases, giving a higher overall order in the porosity. Because the crystallinity is increasing continuously during the polymerization (the polymer is annealing while it is reacting), the diffusivity is continuously decreasing. This is further supported by direct examination of the changing crystal structure. Examination of X-ray–scattering curves for PET (Fig. 10) reveals that the peaks shift to higher scattering angles with an increase in crystallinity (associated with increased time and temperature of annealing). This increase implies smaller spacing between the scattering planes, which in turn, should be connected with increased resistance to diffusion. These considerations makes the small deviations in Figures 8 and 9 understandable while showing that the model assumptions still give reasonable predictions.

As mentioned above, model predictions of intrinsic or inherent viscosity should be compared with the data because the number-average molecular weight derived from viscosity experiments is incorrect if the polydispersity is unknown. In Figure 11, the number-average molecular weights calculated with the solid-state model of this work are compared with the number-average molecular weights obtained by Jabarin et al. from the Mark-Houwink expression. The deviation is clear. Additionally, because the polydispersity increases during the polymerization, the curvature seen in the real number-average molecular weight data is masked. The need for using intrinsic or inherent viscosity (or adjusting for the polydispersity change) is thus apparent.

Another interesting aspect to the modeling of PET solid-state reactions concerns the fraction of end groups that are carboxyl. Because titration of these polymers is so difficult, many of the published works discuss only the change in intrinsic viscosity. But, if one wishes to model these reactions on a molecular level, information on the initial carboxyl fraction must be given. When Ravindranath et al.[12] reworked Chang's data, all end groups were assumed to be hydroxyl. This assumption was tested by fitting diffusion parameters for two different initial conditions: carboxyl end group fractions of 32 and 0% (with all other parameters from Table VI). The large variation in the apparent diffusivity (shown in Table VIII) emphasizes the importance of knowing the initial carboxyl content. The initial carboxyl content was also found by Duh to have considerable influence on the rate of solid-state reaction.[39]

As a further check, the estimated diffusivity for ethylene glycol was compared to literature data for diffusion constants in the melt at 270°C. Table VIII shows the current result is well within the scatter of values.

An ethylene glycol diffusion constant has also been estimated for the solid state by Ravindranath et al.[12] In Table VII, the assumed initial con-

Table VIII Ethylene Glycol Diffusion Constant at 270°C

Conditions	Diffusion Constant (cm^2/s)
Bonatz et al. prediction[40]	0.93×10^{-5}
Extrapolation from solid state (above)	3.1×10^{-5}
Pell and Davis[41]	17.0×10^{-5}
Rafler[42]	0.82×10^{-5}

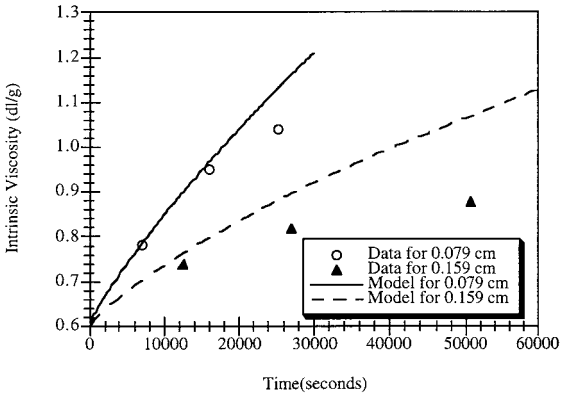

Figure 12 *A priori* prediction of particle size effect at 230°C, data of Chang.[11]

Table IX Parameters for Simulations in Figures 13 and 14

Initial material	Experimental PET, 14000 molecular weight
Initial carboxyl fraction of total end groups	0.156
Particle radius	0.10 cm

centration of carboxyl end groups was shown to greatly affect the estimated diffusivity. Because Ravindranath et al. assumed that all polymer ends were glycol ended, to compare their diffusion constant to the one of this work, the same assumption must be made (second row in Table VII). With a crystallinity of 45% at 220°C, the diffusivity is $D_o(1 - c_c)$ or 2.18×10^{-6} cm^2/s compared to Ravindranath's fitted value of 1.95×10^{-6} cm^2/s. Given that this study has used the data of Jabarin et al.[3] to fit the model while Ravindranath et al. used Chang's data,[11] the fitted diffusivity seems reasonable and consistent. In other words, a model with a small number of fitted constants (two) has been developed that compares well to the data. The constants in this model compare favorably to other independent measurements.

Another assumption that requires discussion is the effect of the degradation rate in polyester systems. Much of the work that has been published on solid-state polycondensation assumes that no degradation reactions are occurring. With the current model, the effect of this assumption was tested in two ways. First, when the degradation reaction was assumed to be negligible, the fitted diffusivity and activation energy were essentially identical to that found with degradation

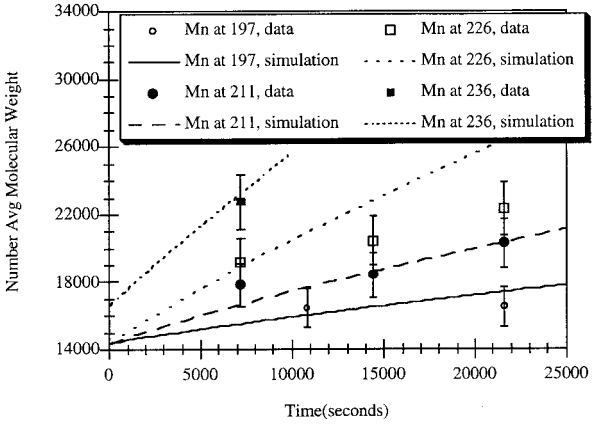

Figure 13 *A priori* prediction of number-average molecular weight, data of this work.

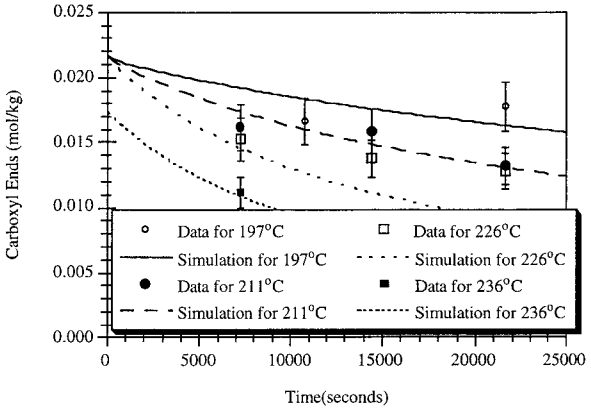

Figure 14 *A priori* prediction of carboxyl ends concentration, data of this work.

reaction calculated explicitly. Second, the rate of degradation at 230°C, with the rate constants of Table III, is 8.4×10^{-6}/h. This means that over the course of 10 h 0.005% of the linkages will be degraded (accounting for crystallinity). Because the total end group concentrations are about 0.05 mol/kg (about 0.5% of the linkage concentration), degradation creates only a small fraction of endgroups (about 1%) at solid-state conditions.

Diffusion-limited polymerizations should show a variation in molecular weight according to the particle size because the particle size affects the ethylene glycol removal rate. Because building molecular weight is of primary interest in industry, the prediction of the particle size effect is critical for using the model to optimize industrial processes. Although Chang[11] does not give some critical information (such as catalyst type and fraction of carboxyl endgroups) necessary to compare our model precisely, the model with the conditions of

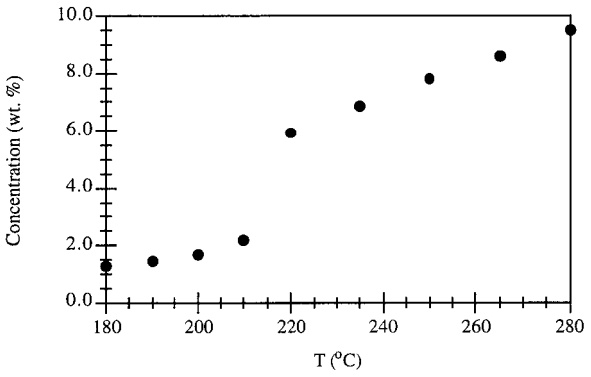

Figure 15 Residual caprolactam in nylon 6, data of Kohan.[43]

Table X Simulation Parameters for Figure 16

Mass transfer	$D_o = 1.20 \times 10^{-6} \exp\left(\frac{-18300}{R}\left(\frac{1}{T} - \frac{1}{475.15}\right)\right)$ cm²/s Diffusivity = $D_o(1 - \chi_c)$ Diffusion is calculated for free water (not total water) Free water is calculated by method of Mallon and Ray[20] Conc. of water = 0 at the particle surface
Particle shape	Spherical
Particle radius	0.16 cm
Initial water content in polymer	1 mol/kg
Crystallinity (χ_c) (found by X-ray scattering)	0.78 for 182 and 202°C polymerizations 0.77 for 226°C polymerization
Kinetics	Mallon and Ray[20]

Table VI estimates the particle size effect well (Fig. 12) (by treating the larger particles as spheres with a radius of 0.159 cm and the smaller particles as spheres with a radius of 0.079 cm).

Our own PET solid-state polymerization experiments determined both the number-average molecular weight and acid end concentration explicitly. Comparisons of these data with the model predictions (using the parameters in Table VI and exceptions in Table IX) are shown in Figures 13 and 14. Because this is a model prediction with parameter fitting, the correspondence of the data with the model seems very good.

NYLON SOLID-STATE POLYMERIZATION—ANALYSIS

Because the fundamental assumptions of our model should also apply to nylon reactions, a discussion of experimental evidence supporting these assumptions is useful. For example, our assumption of small molecules concentrating in the amorphous phase can be tested by examining the data of Kohan[43] on nylon 6. For high conversions, the nylon 6 caprolactam polyaddition equilibrium reaction allows the equilibrium melt concentration of caprolactam to be written as

$$[\mathrm{CL}]_{\mathrm{melt}} = \frac{1}{K_{\mathrm{add}}} \qquad (17)$$

Because the crystallinity for the solid material is on the order of 0.67, and because caprolactam should concentrate in the amorphous phase, our model [eq. (3)] predicts

$$[\mathrm{CL}]_{\mathrm{solid,overall}} = (1 - 0.67)\frac{1}{K_{\mathrm{add}}} \qquad (18)$$

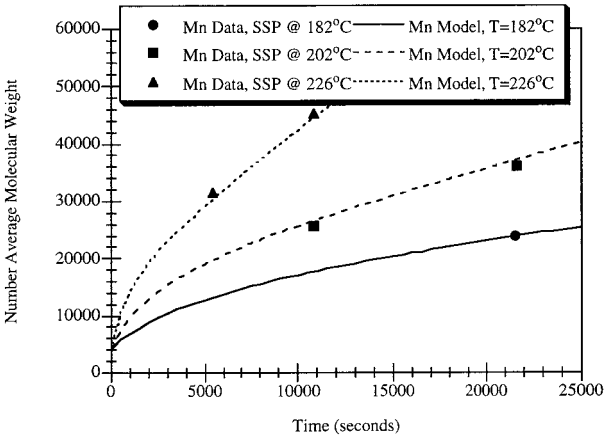

Figure 16 Modeling of solid-state polymerization of nylon 66k, data of this work.

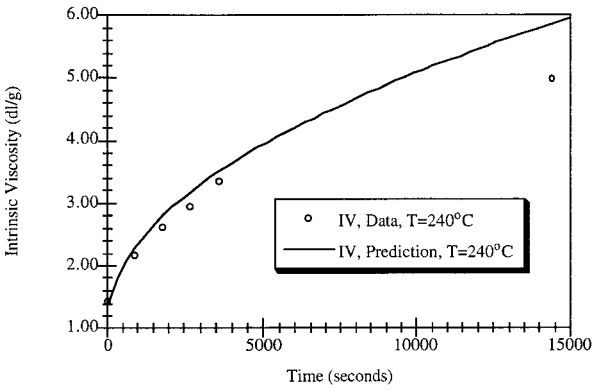

Figure 17 *A priori* model prediction (nylon 66) compared to Srinivasan's data.[45]

Table XI Additional Simulation Parameters for Figure 17

Mass transfer	Diffusivity = 1×10^{-6} $(1 - \chi_c)$ cm^2/s Diffusion calculated for free water (not total water) Free water is calculated by method of Mallon and Ray[20] Conc. of water = 0 at the particle surface
Initial water content in polymer	None
Crystallinity	0.839
Particle shape	Cylindrical
Fiber radius	0.044 cm

Therefore, as nylon 6 melts, our model predicts that the equilibrium caprolactam concentration should triple. The data of Kohan[43] (Fig. 15) show the equilibrium concentration increasing from about 2 to 6% as the nylon 6 melts (between 215 and 220°C); thus supporting this assumption.

NYLON 66 SOLID-STATE POLYMERIZATION—MODELING

This section will first show how the reaction rates of properly crystallized nylon particles are consistent with diffusion limitations (as with PET above). The second part of this section will then show how some particle preparation techniques in the literature have led to mass transfer limits at the particle surface. By accounting for these mass transfer limits, all of the nylon solid-state polymerizations can be understood with our solid-state model.

Nylon experiments carried out in our solid-state reactor were compared with the solid-state model. The model parameters are shown in Table X. To compare the data to the model, only a diffusion coefficient for water was needed. By assuming that the activation energy for diffusion is 18,300 cal/mol (the water sorption energy[44]), only one parameter had to be estimated. This determined the amorphous diffusivity at 202°C as 1.20 $\times 10^{-6}$ cm^2/s. Because only one parameter was fit, the agreement of the model with the data is quite impressive (Fig. 16). The diffusion coefficient is reasonably consistent with a diffusivity determined independently from a TGA desorption: 3.7×10^{-6} cm^2/s (extrapolated from 190°C).

Srinivasan and co-workers[45] carried out a series of interesting experiments on nylon in the solid state. They polymerized nylon fibers and observed the intrinsic viscosity change. Equation (19) (Mark-Houwink constants from Burke and Orofino[46]) was used to convert the viscosity average molecular weight to intrinsic viscosity in a manner identical to that done with PET in eq. (16); the multiplier of M_v is adjusted from the reference to account for the ratio of M_v/M_n for a most probable distribution [as done for eq. (16)].

$$\text{I.V.} = 3.34 \times 10^{-4} M_v^{0.786} \qquad (19)$$

Because nylon fibers are so small, Srinivasan's experiments represent irreversible polyamidation (with no equilibrium limitation). Then, because one of the coauthors of Srinivasan et al. (Knorr[47]) determined the crystallinity of the material under consideration to be 0.839 for reaction at 240°C, the 240°C data can be modeled *a priori* with no adjusted constants (Fig. 17). The simulation parameters are specified in Table X with exceptions

Table XII Additional Simulation Parameters for Figure 18

Mass transfer	Diffusivity = $(2.8 \times 10^{-6}$ cm^2/s$)(1 - \chi_c)$ Diffusion calculated for free water (not total water) Free water is calculated by method of Mallon and Ray[20] Conc. of water = 0 at the particle surface
Initial water content in polymer	0.0
Crystallinity (χ_c)	0.67[48]
Particle size	0.05 cm (sphere radius)

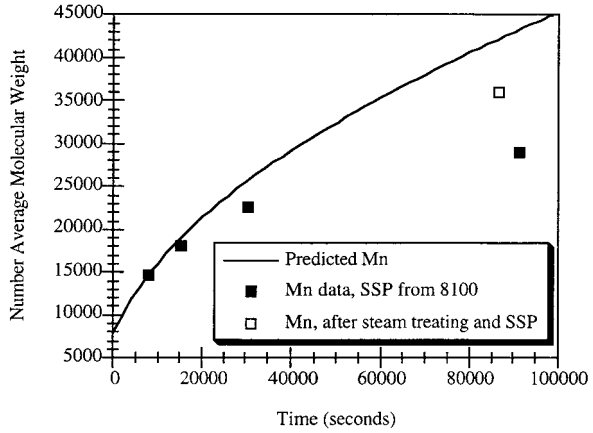

Figure 18 Prediction of molecular weight for data of Gaymans et al.[2] (nylon 6).

and additions in Table XI. Figure 17 shows that the *a priori* prediction is quite reasonable.

As noted above, some nylon solid-state polymerization results exhibit not diffusion limitations but mass transfer limits at the particle surface. Gaymans et al.[2] reported a distinct tendency of nylon solid-state reactions to plateau as higher molecular weights are reached. By contrast, in Figure 16, nylon polymerized in a well behaved fashion from 4000 to about 40,000 molecular weight with no discernible plateau. The reason seems to lie with the pretreatment prior to solid-state polymerization. Gaymans et al.[2] reported increased rates of polymerization when the polymer was steam annealed prior to solid-state reaction (Fig. 18). Superimposed on Figure 18 is the model prediction using the same model as for Figures 16 and 17; parameters are in Table X with exceptions and additions in Table XII. In Figure 18, the model predicts the initial data well. However, at longer times, the steam-annealed particle behaves more like the model prediction than do Gayman's other data. Without more data, one cannot know the difference in the crystalline structure of the two types of particles; however, the water could easily swell and create permanent pores in the solid nylon. Thus, the steam-annealing step is postulated to remove a mass transfer limitation.

The other polymerizations of Gaymans et al. were then modeled assuming no mass transfer because of a diffusion barrier at the particle surface without steam annealing. For each simulation, an initial water content was assumed (Table XIII, with other parameters in Tables X and XII). The polymerization then proceeded without any mass transfer (Fig. 19). By fitting just the initial water content (Table XIII), the model agrees well with the data.

Table XIII Initial Water Concentrations for Simulation

Initial M_n of Experiment	Initial Water Conc. (mol/kg)
2500	0.785
4000	0.564
6300	0.459
8100	0.434
10800	0.191
18300	0.0

CONCLUSIONS

This article has shown the development of a general model to predict PET and nylon solid-state polymerizations. Crystallization-induced fractionation allowed the calculation of apparent kinetics and equilibria with no fitted constants. The model also allowed for the calculation of polymer intrinsic viscosities on a fundamental basis. For PET, the model determined dynamically varying crystallinities that were then coupled to the diffusivity, and mass transfer from the PET pellets was handled in a rigorous fashion. For nylon, polymer particle pretreatment was found to have a great influence on the solid-state behavior. Using a maximum of just two parameters, the model compared favorably with extensive data for PET and nylon.

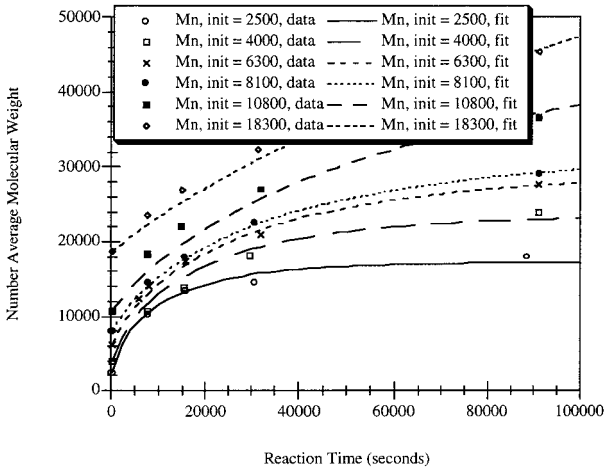

Figure 19 Comparison of model to nylon 6, data of Gaymans et al.[2]

Part II of this series will imbed this particle model into a general model for solid-state polymerization reactors taking into account mixing and residence time distribution issues.

NOMENCLATURE

A_{tot}	total concentration of carbonyl groups (carboxyls and amides)(mol/kg)
C_A	alcohol end conc. (PET) or amine end conc. (nylon)(mol/kg)
$C_{A'}$	vinyl end conc. (PET)(mol/kg)
C_B	carboxyl concentration (mol/kg)
$C_{e.g.}$	concentration of monomeric ethylene glycol (mol/kg)
$C_{amorphous}$	amorphous concentration of a noncrystallizing component such as water
$C_{overall}$	concentration of a noncrystallizing component e.g., water (for the total particle)
$C_{v \text{ or } n}$	concentration of a volatile (v) or nonvolatile (n) component
D_o	diffusivity in completely amorphous polymer
D	diffusivity in semicrystalline polymer
$D_{e.g. \text{ or } w}$	diffusivity of ethylene glycol (e.g.) or water (w)
$f_{solid,v}$	solid phase (amorphous) fugacity of a volatile species
$g_{v \text{ or } n}$	production rate through reaction of a volatile (v) or nonvolatile (n) component in the melt (or amorphous phase)
k_m	mass Transfer Coefficient (moles/s/m^2/torr)
L	concentration of linkages in amorphous phase (each ester or amide bond counts as 1 instead of 0.5 as in notation of Ravindranath et al.)(mol/kg)
M	system mass (kg)
M_v	viscosity average molecular weight
P_i	polymer chain of length i
$R_{v \text{ or } n}$	production rate through reaction of a volatile (v) or nonvolatile (n) component
T	temperature (K)
$w_{i,amorphous}$	weight fractions of the ith component in the designated phase or total
W	water concentration (mol/kg)
W_f	free water concentration (for nylon modeling)(mol/kg)
α	thermal diffusivity
χ_c	mass fraction crystallinity
χ_{max}	maximum crystallinity (mass fraction)
λ_i	ith polymer moment
$\lambda_{1,1}$	conc. of total ethylene glycol (PET) or HMDA (nylon 66) (both free and polymerized)
$\lambda_{1,2}$	conc. of total TPA (PET) or Adipic acid (nylon 66) (both free and polymerized)
ρ	density (kg/L)

REFERENCES

1. F. Pilati, in *Comprehensive Polymer Science,* G. Allen and J. C. Bevington, Eds., Pergamon Press, Oxford, 1989, pp. 201–215.
2. R. J. Gaymans, J. Amirtharaj, and H. Kamp, *J. Appl. Polym. Sci.,* **27,** 2513 (1982).
3. S. A. Jabarin and E. A. Lofgren, *J. Appl. Polym. Sci.,* **32,** 5315 (1986).
4. S. Chen and F. Chen, *J. Polym. Sci., Polym. Chem. Ed.,* **25,** 533 (1987).
5. I. Devotta and R. A. Mashelkar, *Chem. Eng. Sci.,* **48,** 1859 (1993).
6. A. Kaushik and S. K. Gupta, *J. Appl. Polym. Sci.,* **45,** 507 (1992).
7. M. R. Kulkarni and S. K. Gupta, *J. Appl. Polym. Sci.,* **53,** 85 (1994).
8. S. B. Warner and J. Lee, *J. Polym. Sci., Polym. Phys. Ed.,* **32,** 1759 (1994).
9. F. K. Mallon, PhD Thesis, Univ. of Wisc. Madison (1997).
10. F. C. Chen, R. G. Griskey, and G. H. Beyer, *AIChE J.,* **15,** 680 (1969).
11. T. M. Chang, *Polym. Eng. Sci.,* **10,** 364 (1970).
12. K. Ravindranath and R. A. Mashelkar, *J. Appl. Polym. Sci.,* **39,** 1325 (1990).
13. G. Qiu, N. Huang, Z. Tang, and L. Gerking, *Chem. Eng. Sci.,* **52,** 371 (1997).
14. Z. L. Tang, G. Qiu, N. X. Huang, and C. Sironi, *J. Appl. Polym. Sci.,* **57,** 473 (1995).
15. F. K. Mallon and W. H. Ray, *J. Appl. Polym. Sci.,* to appear.
16. D. Patterson and I. M. Ward, *Trans. Faraday Soc.,* **53,** 291 (1957).
17. I. M. Ward, *Trans. Faraday Soc.,* **53,** 1407 (1957).
18. P. G. Kosky, R. S. McDonald, and E. A. Guggenheim, *Polym. Eng. Sci.,* **25,** 389 (1985).

19. K. Ravindranath and R. A. Mashelkar, *AIChE J.,* **30,** 415 (1984).
20. F. K. Mallon and W. H. Ray, *J. Appl. Polym. Sci.,* submitted.
21. S. A. Jabarin, *J. Appl. Polym. Sci.,* **34,** 85 (1987).
22. A. Y. Malkin, V. P. Beghishev, and I. A. Keapin, *Polymer,* **24,** 81 (1983).
23. S. P. Kim and S. C. Kim, *Polym. Eng. Sci.,* **31,** 110 (1991).
24. F. C. Perez-Cardenas, L. F. Del Castillo, and R. Vera-Graziano, *J. Appl. Polym. Sci.,* **43,** 779 (1991).
25. C. Gostoli, F. Pilati, G. C. Sarti, and B. Di Giacomo, *J. Appl. Polym. Sci.,* **29,** 2873 (1984).
26. J. Zimmerman, *J. Polym. Sci., Polym. Lett. Ed.,* **2,** 955 (1964).
27. K. Meyer, *Angew. Makromol. Chem.,* **34,** 165 (1973).
28. H. Fujita, *Fortschr. Hochpol.-Forsch.,* **3,** 1 (1961).
29. A. S. Michaels, W. R. Vieth, and J. A. Barrie, *J. Appl. Phys.,* **1,** 13 (1963).
30. K. H. Yoon, M. H. Kwon, M. H. Jeon, and O. O. Park, *Polym. J.,* **25,** 219 (1993).
31. M. G. Kulkarni and R. A. Mashelkar, *Chem. Eng. Sci.,* **38,** 941 (1983).,
32. C. G. Hill, *An Introduction of Chemical Engineering Kinetics & Reactor Design,* Wiley, New York, 1977.
33. L. L. Jacobsen, PhD Thesis, University of Wisconsin–Madison (1991).
34. P. J. Flory, *J. Am. Chem. Soc.,* **61,** 3334 (1939).
35. D. E. Kokkalas, D. N. Bikiaris, and G. P. Karayannidis, *J. Appl. Polym. Sci.,* **55,** 787 (1995).
36. L. H. Buxbaum, *J. Appl. Polym. Sci.,* **35,** 59 (1979).
37. L. D. Moore, *ACS Meet.,* **1,** 234 (1960).
38. E. L. Lawton and E. L. Ringwald, in *Polymer Handbook,* J. Brandrup and E. H. Immergut, Ed., Wiley, New York, 1989, p. V101.
39. B. Duh, U.S. Pat. to Goodyear #4,238,593 (1979).
40. E. Bonatz, G. Rafler, and G. Reinisch, *Angew. Makromol. Chem.,* **119,** 137 (1983).
41. T. M. Pell and T. G. Davis, *J. Polym. Sci., Polym. Phys. Ed.,* **11,** 1671 (1973).
42. G. Rafler and K. Zacharias, *Acta Polym.,* **31,** 732 (1980).
43. M. I. Kohan, in *Nylon Plastics,* Kohan, Ed., Wiley, New York, 1973, p. 13.
44. O. Fukumoto, *J. Polym. Sci.,* **22,** 263 (1956).
45. R. Srinivasan, P. Desai, A. S. Abhiraman, and R. S. Knorr, *J. Appl. Polym. Sci.,* **53,** 1731.
46. J. J. Burke and T. A. Orofino, *J. Polym. Sci.,* **A-2,** 1 (1969).
47. R. S. Knorr, U.S. Pat. to Monsanto #5,073,453 (1991).
48. D. C. Prevorsek, S. Murthy, and Y. D. Kwon, *Rubber Chem. Technol.,* **60,** 659 (1986).